MECHANIKA
TEORETYCZNA
I STOSOWANA
3-4,28 (1990)

CALCULATION OF LIFT DISTRIBUTION ON CANARD AIRPLANE BY USE VORTEX-LATTICE METHOD

ZDOBYSŁAW GORAJ

WITOLD MOLICKI

Warsaw University of Technology, Warszawa

1. Introduction

Canard configuration possesses the considerable aerodynamic interaction between the front and main wing. Vortices flowing down from the ends of the front wing can considerably disturb the main wing flow. Traditional accounting the average downwash very often is not trustworthy what is involved by very strong change of the induced velocities along the main wing span, especially in the range of end vortices flowing down from the front wing. Taking the above into consideration the classical Vortex Lattice Method [1] was employed to determine the flow around the canard configuration. The superpanel method [2] was used to accounting the deflected flaps, the body, crescent wing and the main wing winglets. The geometrical datas for each panel was coded using computer technic [3]. Lift distributions were obtained and analyzed especially taking into account the dihedral angles and vertical displacement the main wing with respect to the front one. Some aerodynamic characteristics such as gradient $dc_L/d\alpha$ and centre of pressure position were computed. Downwashes behind the front wing and their contours on the yz plane as well as the three-dimensional plots are shown.

2. Integral equation of lifting surface

For steady, potential and subsonic flow of inviscid fluid around the set of small curvature planes the velocity potential function φ satisfies the Laplace equation

$$(1-M^2)\frac{\partial^2\varphi}{\partial x_1^2}+\frac{\partial^2\varphi}{\partial y_1^2}+\frac{\partial^2\varphi}{\partial z_1^2}=0, \tag{2.1}$$

where $K_1x_1y_1z_1$ is a movable set of coordinates, connected with the airplane, whilst K_1 x_1 axis is directed with accordance to the undisturbed flow velocity U_∞ .

Equation (2.1) in the fixed set of coordinates $K_2x_2y_2z_2$ has the form

$$\frac{\partial^2\varphi}{\partial x_2^2}+\frac{\partial^2\varphi}{\partial y_2^2}+\frac{\partial^2\varphi}{\partial z_2^2}=0. \tag{2.2}$$

After the Prandtl-Glauert transformation in the form:

$$x_3=\frac{x_2}{\sqrt{1-M^2}},\quad y_3=y_2,\quad z_3=z_2, \tag{2.3}$$

from the set of coordinates $K_2x_2y_2z_2$ to the movable set of coordinates $K_3x_3y_3z_3$, connected with the wing, equation (2.2) keeps the canonic form

$$\frac{\partial^2\varphi}{\partial x_3^2}+\frac{\partial^2\varphi}{\partial y_3^2}+\frac{\partial^2\varphi}{\partial z_3^2}=0. \tag{2.4}$$

It means that in the new space $K_3x_3y_3z_3$ the dimension $x_3=x_2\beta$ is $\beta=1/\sqrt{1+M^2}$ times greater than the corresponding dimension x_2 , whereas the velocity

$$V_{x3}\frac{\partial\varphi}{\partial x_3}=V_{x2}\partial\beta,$$

is β times less than the velocity V_{x2} .

Solution of the equation (2.4) has form of the single and double layer potential

$$\varphi(x_3,y_3,z_3) = \tag{2.5}$$
$$= \frac{1}{4\pi}\int_S\int\left[\varphi(\xi_3,\ \eta_3,\ \zeta_3)\frac{\partial}{n}\left(\frac{1}{R_3}\right)-\frac{1}{R_3}\frac{\partial}{n}\varphi(\xi_3,\eta_3,\zeta_3)\right]\mathrm{dS},$$

where

$$R_3=\sqrt{(x_3-\xi_3)^2+(y_3-\eta_3)^2+(z_3-\zeta_3)^2}. \tag{2.6}$$

For determination the flow around an aircraft it is necessary to know an influence function $K(x_3,\xi_3;s_3,\sigma_3,M)$, connecting $\mathrm{d}\bar{w}$ and $\mathrm{d}\bar{p}$ between themselves according to relation

$$\mathrm{d}\bar{w}(x_3,s_3)=K(x_3,\xi_3;s_3,\sigma_3,M)\mathrm{d}\bar{p}(\xi_3,\sigma_3), \tag{2.7}$$

where $\bar{w}$, $\bar{p}$ denote dimensionless velocity, normal to lifting surface and dimensionless pressure respectively, i.e.

$$\bar{w}=\frac{w}{U\infty},\quad \bar{p}=\frac{p}{\frac{1}{2}\rho U_\infty^2}, \tag{2.8}$$

whilst (x_3,s_3) and (ξ_3,σ_3) are natural coordinates of collocation and sending point respectively, whereas $\mathrm{d}\bar{w}$ denote elementary velocity normal to lifting surface in

collocation point, induced by the pressure over the elementary surface dS in sending point.

The total normal velocity $\bar{w}(x_3, s_3)$ induced in collocation point $R(x_3, s_3)$ by all sending points $S(\xi_3, \sigma_3)$ is equal:

$$\bar{w}(x_3, s_3) = \int_S \int K(x_3, \xi_3; s_3, \sigma_3, M)\bar{p}(\xi_3, \sigma_3)\mathrm{d}S_3 \tag{2.9}$$

Integral equation (2.9) can be approximated by the linear set of equations:

$$\bar{w}_r = \sum_s D_{rs}\bar{p}_s, \tag{2.10}$$

where:

$$D_{rs} = \int_{S_s} \int K(x_3, \xi_3; s_3, \sigma_3, M)\mathrm{d}S_{s3}.$$

It follows from (2.10) that the velocity w in receiving point R induced by the pressure over the elementary surface $\mathrm{d}S_{s3}$ is equal:

$$\bar{w}_{rs} = D_{rs}\bar{p}_s,$$

or:

$$\frac{w_{rs}}{U_\infty} = D_{rs}\frac{p_s}{\frac{1}{2}\rho U_\infty^2}. \tag{2.11}$$

From Kutta-Żukowski formula the lifting force F_s acting on plane of unit span with horseshoe vortex of circulation Γ_s has the form:

$$F_s = \rho U_\infty \Gamma_s,$$

whereas the pressure over the panel of the mean geometric chord Δx_s is:

$$p_s = \frac{\rho U_\infty \Gamma_s}{\Delta x_s}. \tag{2.12}$$

From (2.11), (2.12) we have:

$$D_{rs} = \frac{w_{rs}\Delta x_s}{2\Gamma_s}. \tag{2.13}$$

The normal velocity w_{rs}, induced in receiving point R by the infinite horseshoe vortex filament Γ_s, was determined using Biot-Savart law.

The total velocity V_i induced in point R by the vortex filament Γ_s of length l (Fig.1) is equal:

$$V_i = \frac{\Gamma_s \times d}{4\pi d^2}(\cos\Theta - \cos\varphi),$$

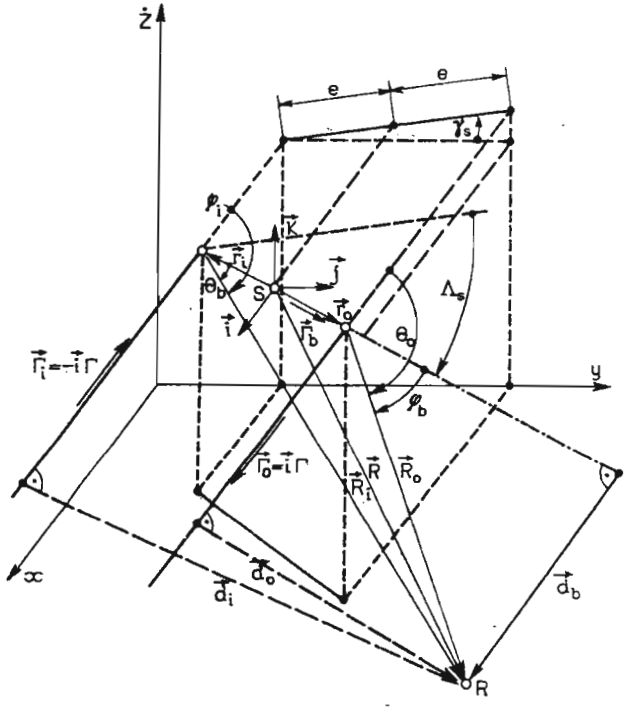

Fig. 1. Geometric relations between horseshoe vortex and the points-sending S and receiving R

whilst velocity w_{rs} is:

$$w_{rs} = \Gamma_s(V_y \sin\gamma_r - V_z \cos\gamma_r), \tag{2.14}$$

whereas

$$\begin{aligned} &\text{a)} \quad V_y = V_{by} + V_{iy} + V_{oy}, \\ &\text{b)} \quad V_z = V_{bz} + V_{iz} + V_{oz}, \end{aligned} \tag{2.15}$$

$$\begin{aligned} \text{a)} \quad V_{by} &= \frac{\cos\Theta_b - \cos\varphi_b}{4\pi d_b^2}(\cos\Lambda_s \sin\gamma_s db_x - \sin\Lambda_s db_z), \\ \text{b)} \quad V_{bz} &= \frac{\cos\Theta_b - \cos\varphi_b}{4\pi d_b^2}(\sin\Lambda_s db_y - \cos\Lambda_s \cos\gamma_s db_y), \end{aligned} \tag{2.16}$$

$$\begin{aligned} \text{a)} \quad V_{iy} &= \frac{R_{iz}(1-\cos\varphi_i)}{4\pi(R_{iy}^2 + R_{iz}^2)} \quad , \quad V_{iz} = \frac{-R_{iz}(1-\cos\varphi_i)}{4\pi(R_{iy}^2 + R_{ix}^2)}, \\ \text{b)} \quad V_{oy} &= \frac{-R_{oz}(1+\cos\Theta_o)}{4\pi(R_{oy}^2 + R_{oz}^2)} \quad , \quad V_{oz} = \frac{R_{oz}(1+\cos\Theta_o)}{4\pi(R_{oy}^2 + R_{oz}^2)}, \end{aligned} \tag{2.17}$$

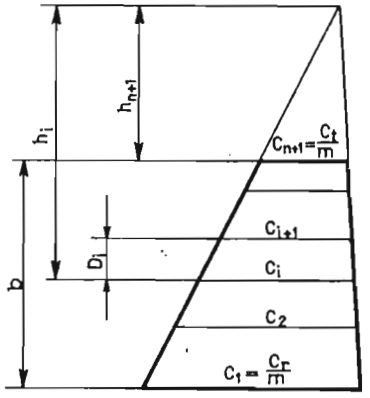

Fig. 2. Geometric relations between the superpanel height b and i-thpanel parameters: chords c_i, c_{i+1} and height D_i

$$\text{a)} \quad \cos\Theta_b = = \frac{1}{R_i}(R_{ix}\sin\Lambda_s + R_{iy}\cos\Lambda_s\cos\gamma_s R_{iz}\cos\Lambda_s\sin\gamma_s),$$

$$\text{b)} \quad \cos\varphi_b = = \frac{1}{R_o}(R_{ox}\sin\Lambda_s + R_{oy}\cos\Lambda_s\cos\gamma_s R_{oz}\cos\Lambda_s\sin\gamma_s), \tag{2.18}$$

$$\cos\varphi_i = -\frac{R_{ix}}{R_i}, \quad \cos\Theta_o = \frac{R_{ox}}{R_o}, \tag{2.19}$$

$$\text{a)} \quad R_{ix} = (x_2 - \xi_2)\beta + e\,\mathrm{tg}\Lambda_s;\ R_{ox} = (x_2 - \xi_2)\beta - e\,\mathrm{tg}\Lambda_s,$$
$$\text{b)} \quad R_{iy} = y_2 - \eta_2 + e\cos\gamma_s;\ R_{oy} = y_2 - \eta_2 - e\cos\gamma_s, \tag{2.20}$$
$$\text{c)} \quad R_{iz} = z_2 - \zeta_2 + e\sin\gamma_s;\ R_{oz} = z_2 - \zeta_2 - e\sin\gamma_s,$$

$$\text{a)} \quad db_x = R_{ix} - R_i\cos\Theta_b\sin\Lambda_s,$$

$$\text{b)} \quad db_y = R_{iy} - R_i \cos\Theta_b \cos\Lambda_s \cos\gamma_s, \tag{2.21}$$

$$\text{c)} \quad db_z = R_{iz} - R_i \cos\Theta_b \cos\Lambda_s \sin\gamma_s,$$

$$R_i = \sqrt{R_{ix}^2 + R_{iy}^2 + R_{iz}^2}; R_o = \sqrt{R_{ox}^2 + R_{oy}^2 + R_{oz}^2}, \tag{2.22}$$

$$d_b = \sqrt{d_{bx}^2 + d_{by}^2 + d_{bz}^2}. \tag{2.23}$$

$\Lambda_s, \gamma_s, \gamma_r$ denote sweep and dihedral angle in sending point and dihedral in receiving point respectively.

Substitution (2.14) into (2.13) gives

$$D_{rs} = \frac{\Delta x_s (V_y \sin\gamma_r - V_z \sin\gamma_r)}{2}. \tag{2.24}$$

3. Lifting surface division into superpanels

It was assumed that the lifting surface can be divided into finite number of trapezoidal elements socalled superpanels. This super panels are adjusted to leading edges, trailing edges, hinge axis and other border lines. This division can be arbitrary but of course the number of superpanels should be as small as possible. Each superpanel is next divided into trapezoidal boxes, socalled panels. The error of computation of the lift distribution will be minimized if the division of the surface into panels is such that these panels have aspect ratio of order unity. Division into panels can be made with aid of computer if we know the number of elements in chord as well as in span directions (Fig.2). It was assumed that unknown aspect ratio λ of each panel in an arbitrary superpanel can be computed as a function of chords c_i, c_{i+1} and height D_i in the form $\lambda = 2D_i/(c_i + c_{i+1})$. From geometrical considerations follows that $c_i/h_i = c_{i+1}/h_{i+1}$ and that the panel height is

$$D_i(\lambda) = \frac{\lambda c_i}{1 + \frac{\lambda(c_r - c_t)}{2b}} \tag{3.1}$$

The aspect ratio λ can be computed as a solution of the nonlinear equation:

$$\sum_i D_i(\lambda) - b = 0. \tag{3.2}$$

4. Numerical results

Numerical calculations of lift distribution were done for the canard configuration (Fig.3) in many different cases. The front wing has constant section GAW-1,

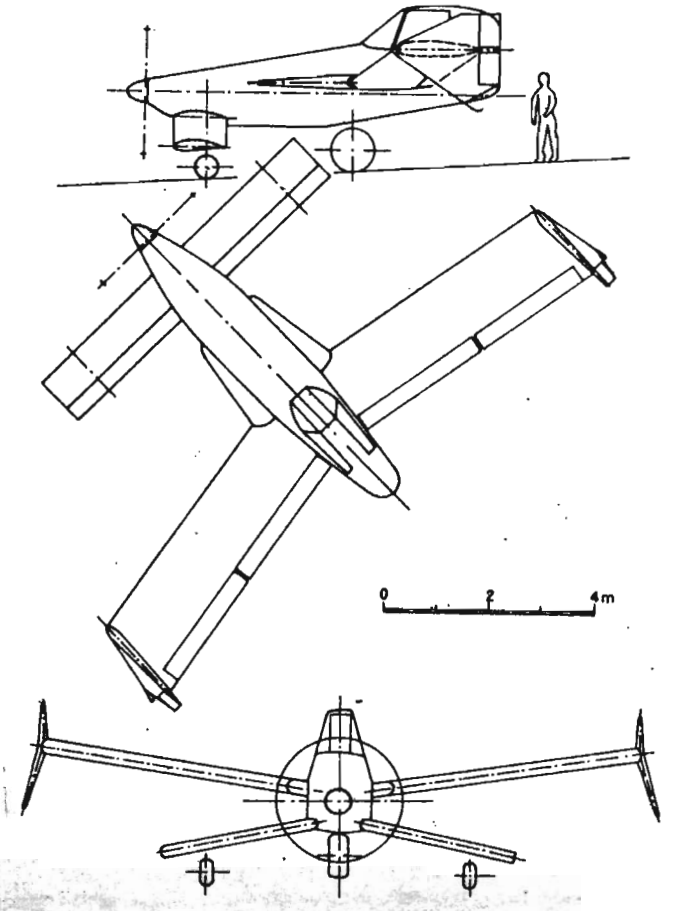

Fig. 3. Plan view of the aircraft, for which the computations was performed

the main one has NACA 63A416. Fig.4 - 6[1] show the lift distribution on the single, isolated main wing, having different sweep angle ($-10°$, $0°$, $+10°$), for the case if dihedral angle is equal to zero. The wing was divided into $m = 8$ and $n = 48$ panels along the chord and span respectively. When the sweep angle increases from negative to positive values one can observe

— an increasing of the lift force coefficient (from 0.765, through 0.797 up to 0.806),

— a shifting back of the centre of pressure (from 0.880, through 0.988 up to 1.099

[1]The figures at the end of the paper

[m]),

— a side shifting of the centre of pressure of half wing from the root to the tip (from 0.631, through 0.638 up to 0.647 [m]),

— a shifting back of the nose of the mean aerodynamic chord (from 0.733, through 0.862 up to 0.990 [m]).

Fig.7 shows the lift distribution on the single main wing with body elements. The total number of panels is 588. An local increasing of pressure on leading edge in the immediate vicinity of the body is caused by the sawtooth on the leading edge of the set body-wing and, in consequence, by vortices curling from the down to the up side of surface of the body. Although the lifting surface as a whole increased, so the lifting force coefficient c_L , related to the same wing surface as in Fig.4 - 6, decreased from 0.806 in Fig.6 to 0.794 in Fig.7. Fig.8 - 13 show the lift distribution on wings, fore-wing and body of the canard configuration as a whole. These figures differ between themselves on the front (FD) as well as on the main wing dihedral (MD) and on the vertical displacement one wing with respect to other (VD). Each value of FD, MD, VD can be equal to 0 or 1 . Value 0 denotes that the corresponding parameter is equal to zero
(e.g. FD=0 denotes that the front wing dihedral is equal to zero), whereas value 1 denotes that this parameter is equal to its nominal value, selected by the designer. The nominal values are: $FD = -13.5^o$, $MD = 8^o$, $VD = 0.2$m . Moreover in Fig.8-13 there are printed: the angle of attack of the front wing α(ALFA), the lifting force coefficient of the main wing c_L (CL) and longitudinal as well as the side position of the centre of pressure for the half aircraft: x_{CP} (X CP) and y_{CP} (Y CP). The aircraft as a whole was divided into 44 superpanels, distributed in 14 bands. The bands and superpanels were fitted to flaps, body and fore-wing geometry. The total number of panels is 980. The body is approximated by a thin wing, socalled equivalent body, the shape of which is equal to the projection of the aircraft body on xy surface. Because the wings are displaced one with respect to the other in vertical, so the equivalent body is bent up at the front wing trailing edge and is bent down at the main wing leading edge (Fig.14). For calculating lift distribution it was assumed that local angles of attack in the equivalent body area are equal to zeros, so the obtaining pressure (in body area) should be considered as a influence of wings and fore-wing on the equivalent body. It is pure interference result. Although the arrangement on Fig.13 possesses the greatest lifting force coefficient ($c_L = 0.714$), so it is not acceptable because of very unequal lift distribution along the span, especially because of the pressure concentration in aileron areas. The arrangement on Fig.8 is the most uncoupled and has almost uniform lift distribution over the main wing span. From the longitudinal stability point of view the arrangement on Fig.9 ($x_{CP} = 0.712$m) is the most advantageous, because the centre of pressure is far behind.

After calculating lift distribution on the front wing it is possible to compute

downwashes ϵ in the main wing area using the formula

$$\epsilon_i = \frac{w_i}{U_\infty} = \sum_{j=1}^{n_p} D_{ij}\bar{p}_j = \sum_{j=1}^{n_p} D_{ij}\frac{p_j}{\frac{1}{2}\rho U_\infty^2}, \tag{4.1}$$

where n_p is the number of panels on the front wing.

Calculating downwashes ϵ have been made on a grid $n = 60$ points along the span and $l = 20$ points in the z direction, perpendicular to wing span. Fig.15 and 17 show numerical results for the case, when the front wing dihedral is equal to zero. Fig.16 and 18 show the same for case, when the front wing dihedral is equal to -13.5^o . Fig.15-16 contain the downwashes contours in yz plane, Fig.16-18 show the corresponding three-dimensional plots of these downwashes as functions $\epsilon[y/(b/2), z/(b/2)]$. All Fig.15-18 are symmetric with respect to the z axis, what is caused by symmetric geometry and symmetric flow with respect to the symmetry plane of the aircraft. Tip vortices flowing down from the front wing change the positive downwashes (what means decreasing of the effective angles of attack on the main wing) for $|2y/b| < 1$ on negative downwashes (what means increasing of the effective angles of attack on the main wing) for $|2y/b| > 1$. The negative dihedral of the front wing enables to decouple both the wings aerodynamically, without the necessity of vertical shifting the main wing with respect to the front one. It can be concluded from Fig.16, 18, where the areas of maximum downwashes (inside the contour with the value equal to (4.1) in Fig.16 and both maximum convexities in Fig.18) are shifted down, below the main wing position. Fig.16, 18 correspond to the arrangement from Fig.8, for which we can observe conspicuous equalization of the pressure over the main wing span, whereas Fig.15, 17 correspond to the arrangement from Fig.13, which is the most aerodynamically coupled.

5. Final remarks

Superpanel version of the classical Vortex Lattice Method presented here enables calculating lift distribution for complex geometry as well as including an equivalent body into computations. It is especially important and convenient for strongly aerodynamically coupled configurations, in that for canard aircraft. In such case the separate calculating lift distribution on the front and main wing is not necessary. All interference effects will be included. The method enables to design such the geometric configuration, which can possess the requested aerodynamic properties (e.g. request that lift distribution over the main wing span might be approximately constant). Deflected flaps, slats, winglets, wingtip fins or other lifting surfaces can be easily included into analysis. Downwashes distribution on the main wing for canard configuration or on horizontal tail for classic configuration can be simply calculated and analyzed.

References

1. S.G.HEDMAN, *Vortex Lattice Method for Calculation of Quasi Steady State Loadings on Thin Elastic Wings* ,Rep.105, Oct.1965,Aeronautical Research Institute of Sweden

2. Z.GORAJ,W.MOLICKI,Z.PATURSKI, *Modelling of the Pressure Distribution on Lifting Surfaces Using the Superpanel Method* ,Proceedings 27th Symposium Modelling in Mechanics, Gliwice 1988, (in Polish) ,pp.177-184

3. Z.GORAJ,W.MOLICKI, *An Automatical Coding of Geometrical Data of an Aircraft for Calculating Lift Distribution on Lifting Surfaces* , Proceedings of the 2nd Polish Conference Microcomputers in Mechanics , Warszawa-Jabłonna 1988, (in Polish)

Streszczenie

W pracy przedstawiono superpanelową wersję klasycznej metody VLM, która umożliwia obliczanie rozkładów ciśnień dla układów silnie sprzężonych aerodynamicznie, w tym również dla układu kaczka. Metoda pozwala na zaprojektowanie konfiguracji geometrycznej samolotu o zadanych z góry parametrach (umożliwia np. spełnienieżądania, aby rozkład ciśnienia wzdłuż rozpiętości płata głównego dla układu kaczka był w przybliżeniu równomierny). Szczególną uwagę poświęcono obliczeniu rozkładów kątów odchylenia strug zapłatem przednim. Przedstawiono izolinie oraz trówymiarowe wykresy kątów odchylenia strug na płaszczyźnie prostopadłe do prędkości opływu niezaburzonego dla różnych konfiguracji geometrycznych samolotu.

Резюме

В работе представлен метод разделения несущих поверхностей на суперпанели. Всякая суперпанель, в свою очередь, может быть разделена на меньшие элементы — панели, при этом удлиннение близкое к единице является наилучшим. Представлены результаты вычисления для самолета системы "утка". Особое внимание обращено на задачу определения угла отклонения потока за передним крылом и выбор такой геометрической конфигурации, при которой распределение давления по размаху крыла является приблизительно постоянным.

Praca wpłynęła do Redakcji 12 października 1988 roku

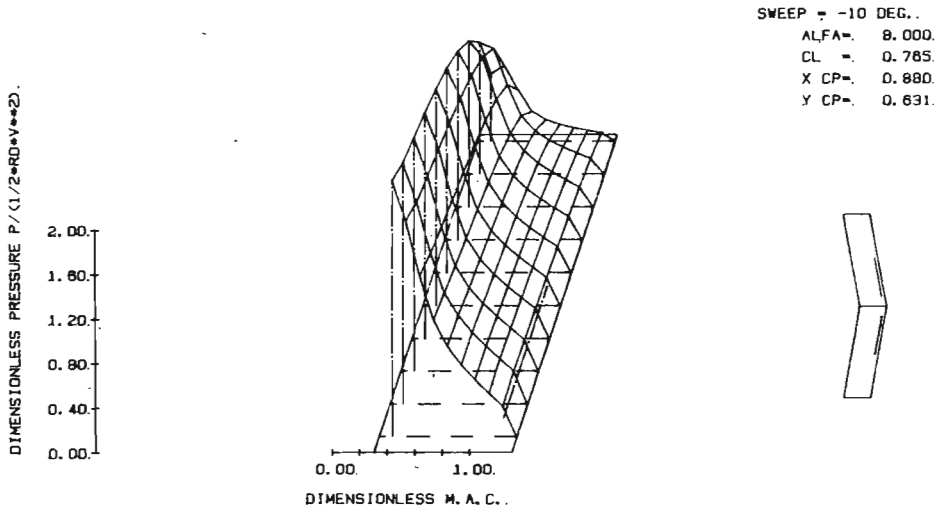

Fig. 4. Lift distribution over the main, isolated half-wing for the case of negative sweep angle

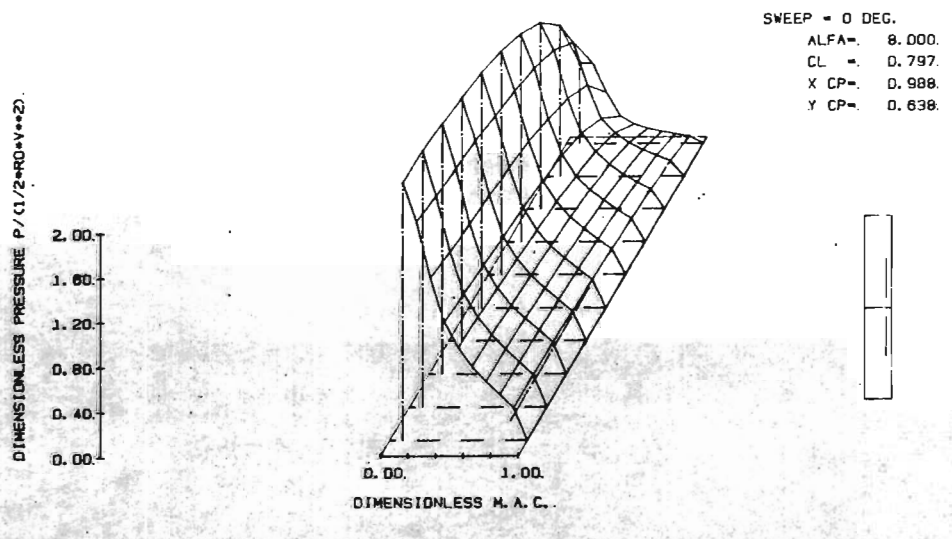

Fig. 5. Lift distribution over the main, isolated half-wing for the case of zero sweep angle

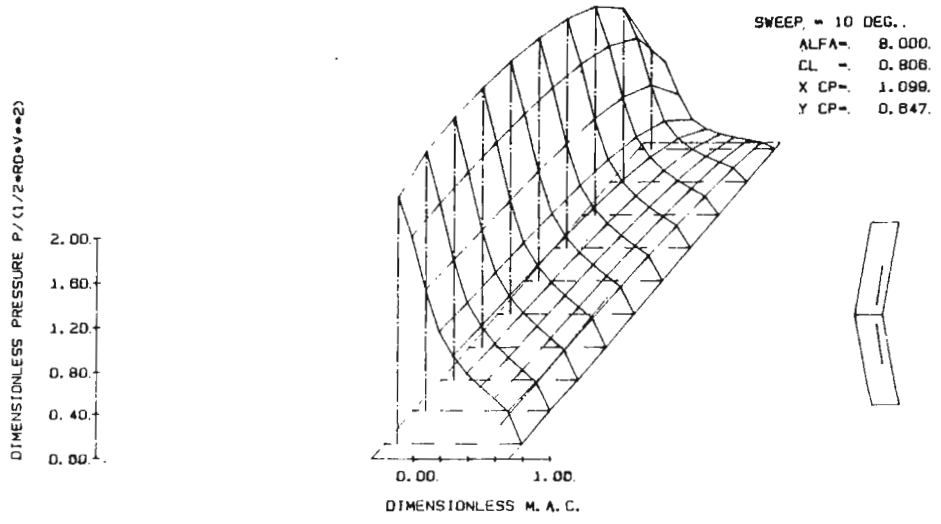

Fig. 6. Lift distribution over the main, isolated half-wing for the case of positive sweep angle

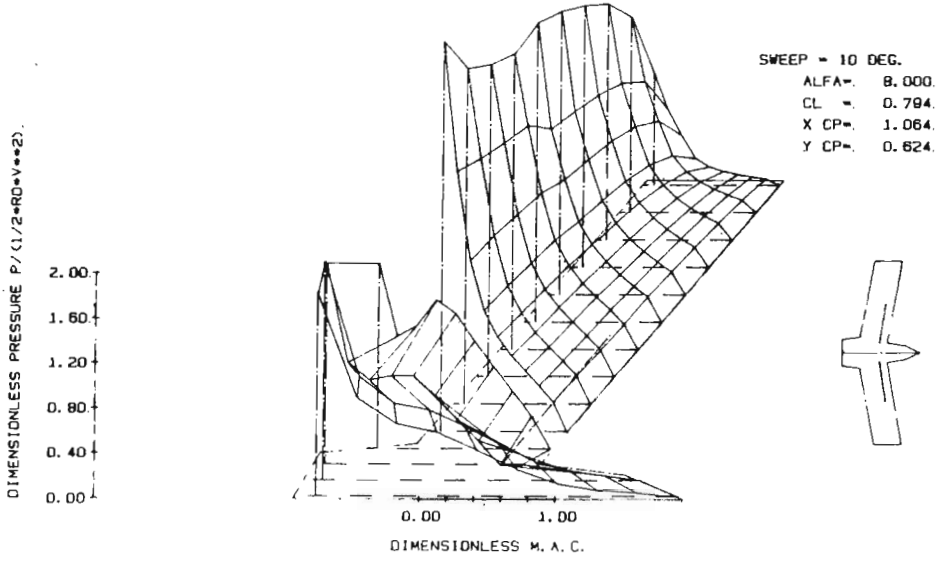

Fig. 7. Lift distribution over the main half-wing with body elements for the case of positive sweep angle

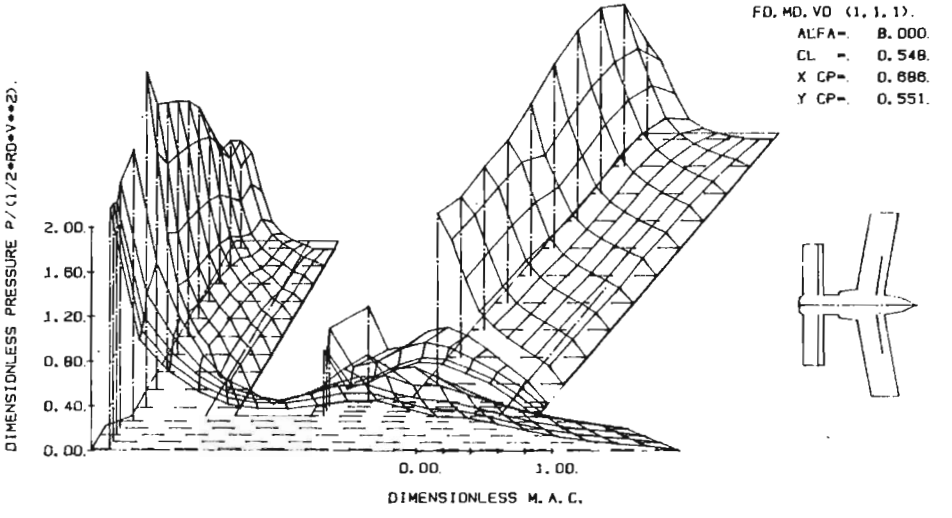

Fig. 8. Lift distribution over the whole half-aircraft for $FD = 1, MD = 1, VD = 1$ (The most coupled case)

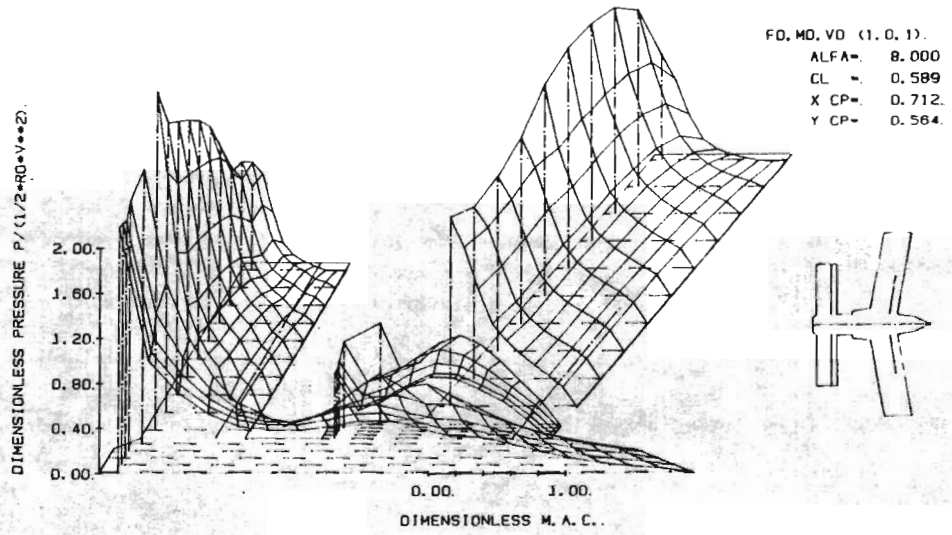

Fig. 9. Lift distribution over the whole half-aircraft for $FD = 1, MD = 0, VD = 1$

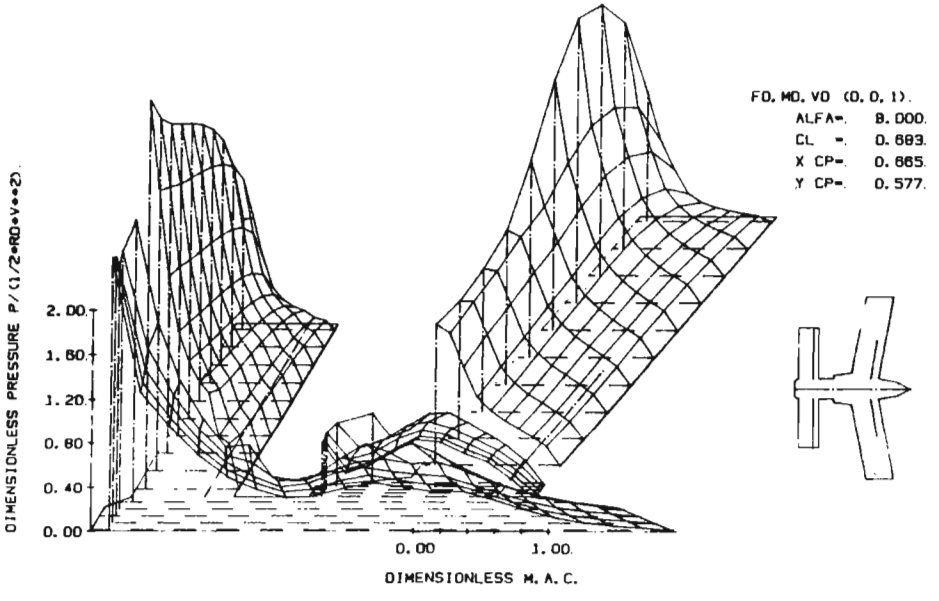

Fig. 10. Lift distribution over the whole half-aircraft for $FD = 0, MD = 0, VD = 1$

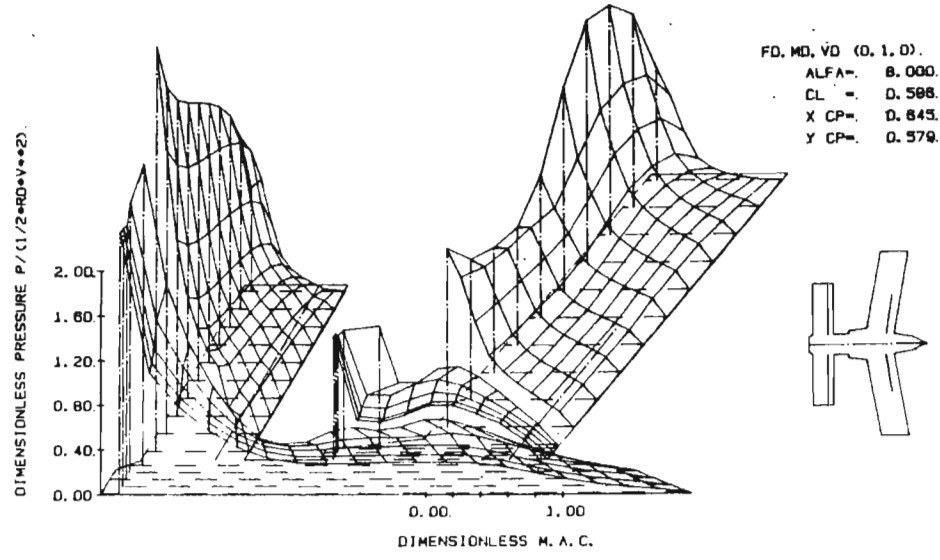

Fig. 11. Lift distribution over the whole half-aircraft for $FD = 0, MD = 1, VD = 0$

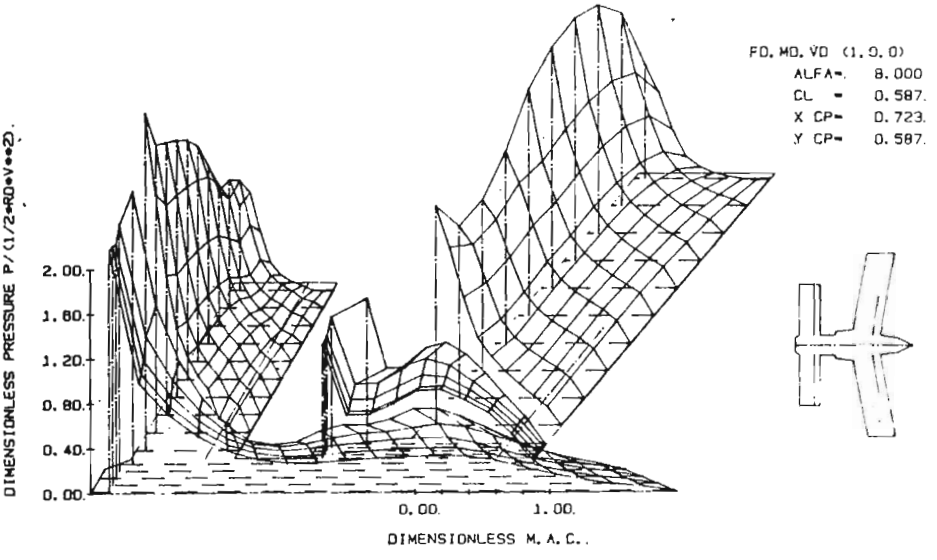

Fig. 12. Lift distribution over the whole half-aircraft for $FD = 1, MD = 0, VD = 0$

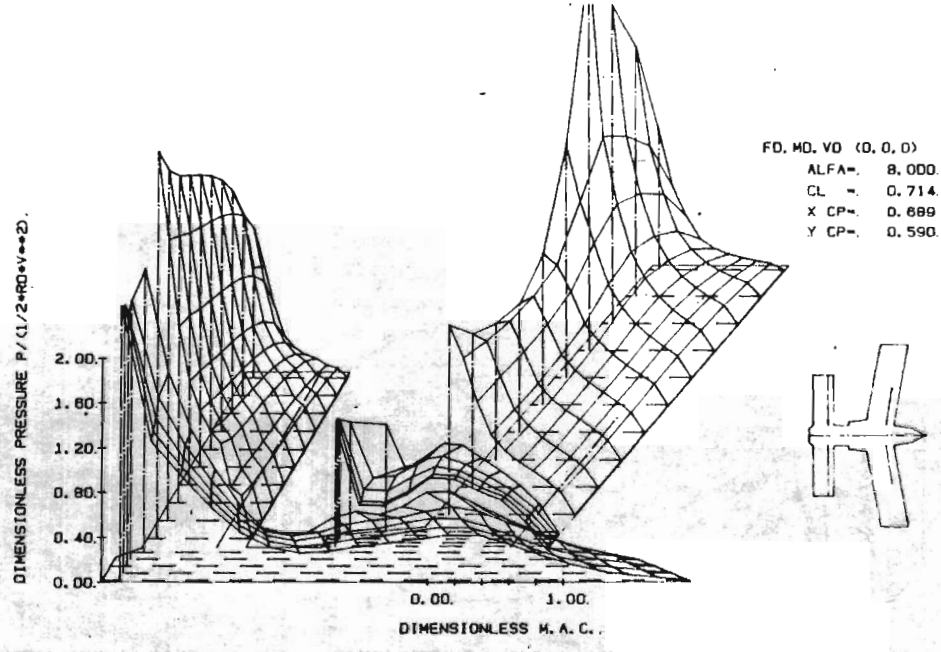

Fig. 13. Lift distribution over the whole half-aircraft for $FD = 0, MD = 0, VD = 0$ (The most uncoupled case)

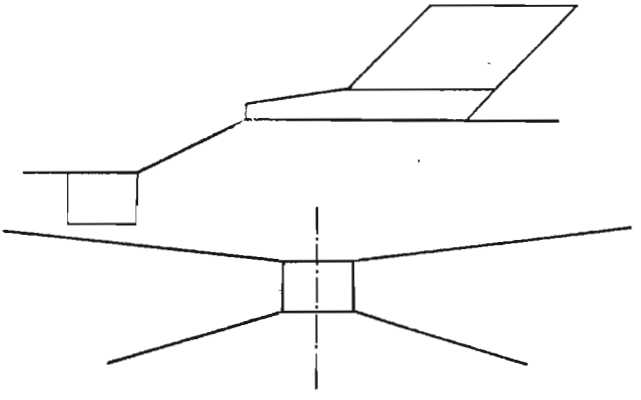

Fig. 14. Plan view of the equivalent body, fore-wing and both the wings

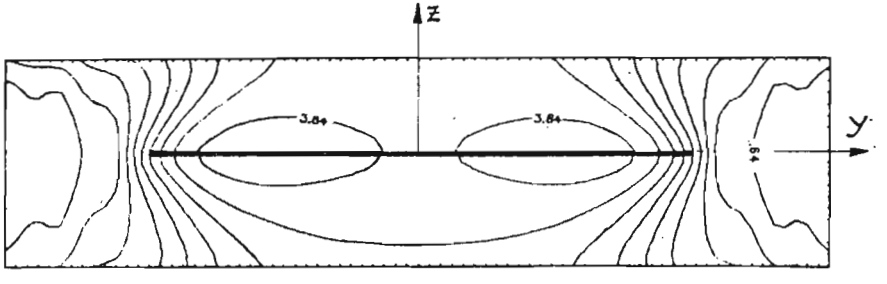

Fig. 15. Downwash contours in the area of the main wing for the case, when the front wing dihedral is equal to zero

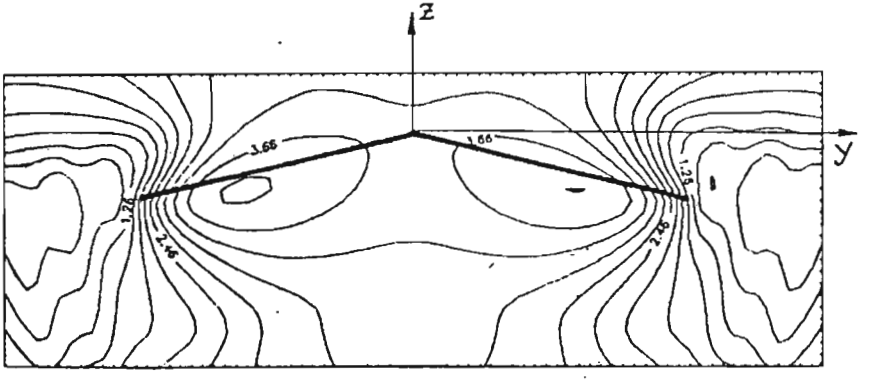

Fig. 16. Downwash contours in the area of the main wing for the case, when the front wing dihedral is negative

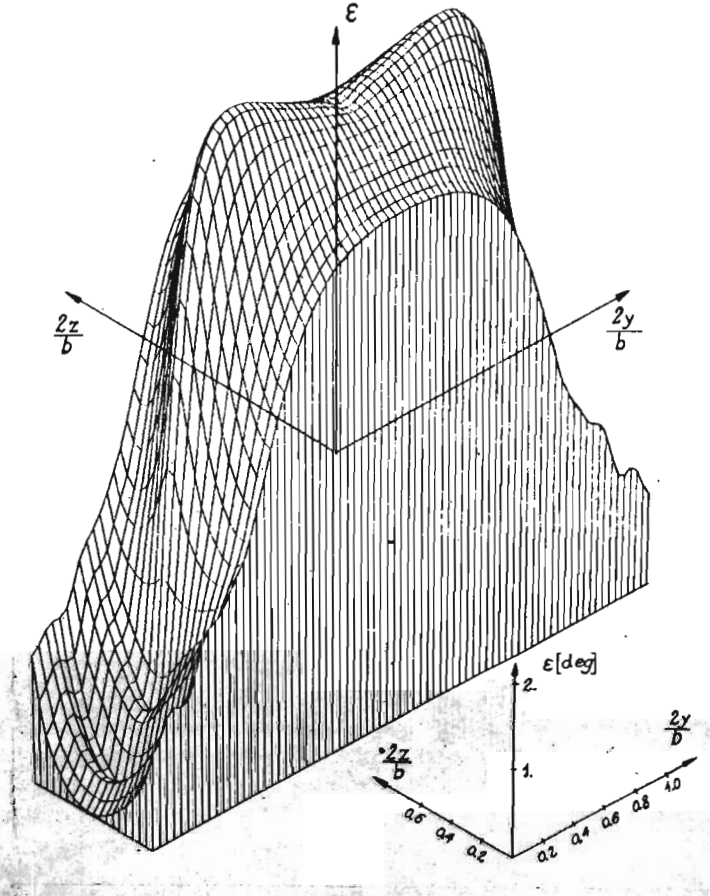

Fig. 17. Downwashes in the area of the main wing as three-dimensional plots for the case, when the front wing dihedral is equal to zero

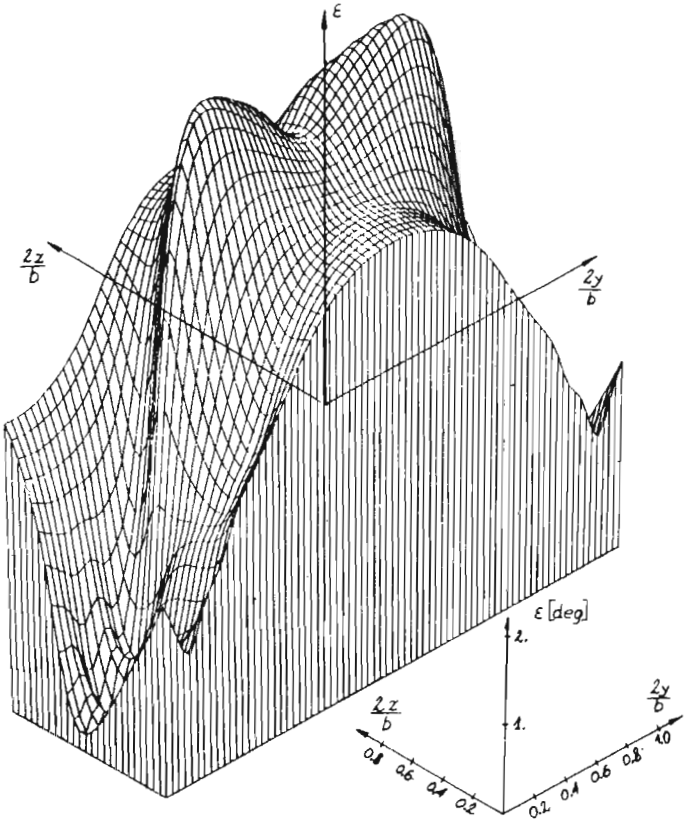

Fig. 18. Downwashes in the area of the main wing as three-dimensional plots for the case, when the front wing dihedral is negative